ResearchGate

See discussions, stats, and author profiles for this publication at: https://www.researchgate.net/publication/325756052

Enriched Galerkin finite elements for coupled poromechanics with local mass conservation

Article *in* Computer Methods in Applied Mechanics and Engineering · December 2018

CITATIONS
0

READS
26

2 authors:

Jinhyun Choo
The University of Hong Kong
26 PUBLICATIONS **157** CITATIONS
SEE PROFILE

Sanghyun Lee
Florida State University
18 PUBLICATIONS **106** CITATIONS
SEE PROFILE

Some of the authors of this publication are also working on these related projects:

Unstable miscible flows in porous media: A survey of analytical and variational numerical methods. View project

(NSF Award Abstract #1546553) BIGDATA: Collaborative Research: IA: F: Fractured Subsurface Characterization using High Performance Computing and Guided by Big Data View project

All content following this page was uploaded by Jinhyun Choo on 14 June 2018.

The user has requested enhancement of the downloaded file.

Enriched Galerkin finite elements for coupled poromechanics with local mass conservation

Jinhyun Choo[a,*], Sanghyun Lee[b]

[a] *Department of Civil Engineering, The University of Hong Kong, Pokfulam, Hong Kong*
[b] *Department of Mathematics, Florida State University, Tallahassee, FL 32306, United States*

Abstract

Robust and efficient discretization methods for coupled poromechanical problems are critical to address a wide range of problems related to civil infrastructure, energy resources, and environmental sustainability. In this work, we propose a new finite element formulation for coupled poromechanical problems that ensures local (element-wise) mass conservation. The proposed formulation draws on the so-called enriched Galerkin method, which augments piecewise constant functions to the classical continuous Galerkin finite element method. These additional degrees of freedom allow us to obtain a locally conservative and nonconforming solution for the pore pressure field. The enriched and continuous Galerkin formulations are compared in several numerical examples ranging from a benchmark consolidation problem to a complex problem that involves plastic deformation due to unsaturated flow in a heterogeneous porous medium. The results of these examples show not only that the proposed method provides local mass conservation, but also that local mass conservation can be crucial to accurate simulation of deformation processes in fluid-infiltrated porous materials.

Keywords: enriched Galerkin method, finite element method, coupled poromechanics, local mass conservation

1. Introduction

In porous materials such as soils and rocks, flow of the pore fluid can give rise to significant deformation of the solid matrix, and vice versa. These poromechanical interactions are central to many important problems that relate to civil engineering [1–6], energy resources [7–10], and environmental sustainability [11–18]. Mathematically, a poromechanical problem is described by a coupled system of two partial differential equations: (1) the linear momentum balance equation which governs the solid deformation, and (2) the mass balance equation which governs the fluid flow. Numerical methods for this coupled system is the focus of the present paper.

The continuous Galerkin (CG) finite element method is one of the most widely used methods to numerically solve a coupled poromechanical formulation (*e.g.,* [19–38]). The use of the CG

*Corresponding Author
Email addresses: jchoo@hku.hk (Jinhyun Choo), lee@math.fsu.edu (Sanghyun Lee)

method for both mass and momentum balance equations has a number of desirable consequences, including its capabilities for handling domains of complex geometry. However, it is well known that the CG method does not guarantee local (element-wise) mass conservation in fluid flow problems, which could lead to inaccurate solutions manifesting non-physical oscillations and/or sub-optimal convergence [39–46]. This aspect is particularly critical for problems that involve markedly heterogeneous permeability fields, sharp interfaces between fluid phases, and coupling with transport phenomena. Since these problems are common in real-world applications, one often needs a more robust and accurate numerical method for coupled poromechanics.

Thus, a locally conservative method is necessary to address the aforementioned problems of the CG method. Locally conservative methods that have been proposed, studied, and used in the poromechanics literature include the finite volume method (*e.g.,* [47–50]), the mixed finite element methods (*e.g.,* [51–54]), and the discontinuous Galerkin (DG) finite element methods (*e.g.,* [55]). Nevertheless, it still remains very challenging to obtain a high order and locally conservative solution without adding significant costs to the CG method. For example, when a DG or a mixed finite element method is used for the same mesh, the number of unknowns for the fluid flow problem can increase several times from its CG counterpart. Such a dramatic increase in the size of the fluid flow problem can be detrimental to the applicability of computational poromechanics, since the large number of unknowns for the solid deformation problem already give rise to significant computational costs.

Over the past years, the enriched Galerkin (EG) finite element method has received growing attention as a locally conservative method with substantially fewer degrees of freedom in comparison with the DG method for a fixed mesh [56–58]. The EG method uses the same bilinear form as the DG method, but it only adds piecewise constant functions to the finite element space of the CG method. For the same polynomial order for approximations, the numerical solutions of the EG and DG methods are very similar, and their optimal rates of error convergence are identical [57, 58]. In this regard, the EG method attains the salient advantages of the DG method with minimal costs added to the CG method. Recently, a class of EG methods have been successfully applied to flow and transport problems in porous media [59–62]. The performance and efficacy of the EG method demonstrated in these studies appear to be promising for addressing the aforementioned challenges in computational poromechanics. Yet, to the best of our knowledge, the application of the EG method to poromechanical problems has not been investigated in the literature.

In this paper, we introduce an EG finite element formulation for locally mass conservative solutions of coupled poromechanical problems. The remainder of the paper proceeds as follows. After brief review of the poromechanical formulation of interest, we develop its numerical approximation whereby the mass balance equation is discretized by the EG finite element method. Subsequently, we study the accuracy and performance of the proposed numerical method through numerical examples ranging from a verification problem to a simple demonstration problem to a complex engineering problem.

The following notations and symbols are used throughout: bold-face letters denote tensors and vectors; the symbol "$\cdot$" denotes an inner product of two vectors (*e.g.,* $\boldsymbol{a} \cdot \boldsymbol{b} = a_i b_i$), or a single contraction of adjacent indices of two tensors (*e.g.,* $\boldsymbol{c} \cdot \boldsymbol{d} = c_{ij} d_{jk}$); the symbol ":" denotes an inner product of two second-order tensors (*e.g.,* $\boldsymbol{c} : \boldsymbol{d} = c_{ij} d_{ij}$). Following the standard mechanics sign convention, stress is positive in tension and pressure is positive in compression.

2. Poromechanical formulation

In this section, we briefly review the balance laws and constitutive models for poromechanics, and state the initial-boundary value problem of our interest.

2.1. Balance laws

Using mixture theory we conceptualize an unsaturated porous material as a three-phase continuum composed of the solid matrix, water, and air. The derivation of balance laws for this type of continuum mixture is well described in the literature (*e.g.,* [25, 63, 64]), so it is not repeated herein. We simply note that the following assumptions are made for arriving at a reasonably simple mathematical model:

1. The mixture is under quasi-static condition.
2. The mixture is free of thermal, chemical, and other complicated effects.
3. The solid deformation is infinitesimal.
4. The solid and water phases are incompressible.
5. The air pressure is atmospheric (passive air condition).
6. The solid and fluid phases do not exchange their masses.

These assumptions are realistic for most problems in shallow subsurface systems. It is noted that the assumption of constant air pressure allows us to neglect the balance of air mass in unsaturated flow, as in the Richards equation.

The coupled poromechanical process is described by two balance laws. The first balance law is for the linear momentum of the mixture, given by

$$\nabla \cdot \boldsymbol{\sigma} + \rho \boldsymbol{g} = \mathbf{0}\,, \tag{1}$$

where $\boldsymbol{\sigma}$ is the total stress in the mixture, ρ is the density of the mixture, and $\boldsymbol{g}$ is the gravitational acceleration vector. The mixture density ρ can be calculated as $\rho = (1-\phi)\rho_s + \phi\rho_w$, where ϕ is the porosity, and ρ_s and ρ_w are the density of the solid and water phases, respectively. The second balance law is for the mass of the pore water, which can be written as

$$\phi\dot{S} + S\,\nabla \cdot \dot{\boldsymbol{u}} + \nabla \cdot \boldsymbol{q} = 0\,, \tag{2}$$

where S is the water-phase saturation, $\boldsymbol{u}$ is the solid displacement vector, and $\boldsymbol{q}$ is the seepage flux vector. The overdot denotes the material time derivative following the motion of the solid matrix.

2.2. Constitutive models

To close the formulation, we introduce three types of constitutive models. The first type is for the solid deformation response. We postulate that the principle of effective stress holds for unsaturated porous materials, and adopt the following form of the effective stress tensor $\boldsymbol{\sigma}'$:

$$\boldsymbol{\sigma} = \boldsymbol{\sigma}' - Sp\mathbf{1}\,, \tag{3}$$

where p is the pore water pressure. Notably, this form of effective stress has been shown to be thermodynamically consistent in the sense that it is energy-conjugate to the rate of deformation tensor of the solid matrix [64]. Then we introduce an effective stress–strain relation for the solid matrix, given by

$$\dot{\boldsymbol{\sigma}}' = \mathbb{C} : \dot{\boldsymbol{\varepsilon}} \,. \tag{4}$$

Here, $\boldsymbol{\varepsilon}$ is the infinitesimal strain tensor, which is related to $\boldsymbol{u}$ as

$$\boldsymbol{\varepsilon} := \nabla^{\mathrm{s}} \boldsymbol{u} = \frac{1}{2}\left(\nabla \boldsymbol{u} + \nabla^{\mathsf{T}} \boldsymbol{u}\right), \tag{5}$$

where ∇^{s} denotes the symmetric gradient operator. Also, $\mathbb{C}$ is the fourth-order tensor of tangent moduli whose specific form depends on the constitutive model for solid deformation. The tangent moduli of common elastoplastic models are explained in [65–67]. It is noted that the above stress–strain relation (4) is expressed in a rate form to include a nonlinear constitutive model such as an elastoplastic model.

The second type of constitutive model is introduced for the seepage flow. Here we use the multiphase extension of Darcy's law, written as

$$\boldsymbol{q} = -\frac{k_{rw}\boldsymbol{k}}{\mu_w} \cdot \left(\nabla p - \rho_w \boldsymbol{g}\right), \tag{6}$$

where k_{rw} is the relative permeability of the water phase, μ_w is the the dynamic viscosity of water, and $\boldsymbol{k}$ is the absolute permeability tensor. In case of isotropic permeability, $\boldsymbol{k}$ reduces to a scalar k_i such that $\boldsymbol{k} = k_i \mathbf{1}$. For notational convenience, we define a lumped permeability tensor $\boldsymbol{\kappa} := (k_{rw}/\mu_w)\boldsymbol{k}$.

Lastly, for unsaturated cases, we introduce a constitutive model that links the water saturation with the pore water pressure. Our particular choice is the van Genuchten model [68], which can be expressed as

$$S = S_1 + (S_2 - S_1)\left[1 + (-p/s_\alpha)^a\right]^{-b}, \tag{7}$$

where S_1 and S_2 are the residual and maximum saturations, respectively, s_α is the scaling suction, and a and b are the exponent parameters in the van Genuchten model. These exponent parameters are related as $b = (a-1)/a$. The van Genuchten parameters can also be used for determining the relative permeability as follows:

$$k_{rw} = S_e^{1/2}\left[1 - (1 - S_e^{1/b})^b\right]^2, \quad S_e = (S - S_1)/(S_2 - S_1)\,. \tag{8}$$

Once the above constitutive models are inserted into the two balance equations (1) and (2), the problem has two unknowns, namely the solid displacement $\boldsymbol{u}$ and the pore pressure p. This leads to the so-called $\boldsymbol{u}/p$ formulation described in the following.

2.3. Initial-boundary value problem statement

We now state an initial-boundary value problem for the coupled poromechanical process. Let $\Omega \in \mathbb{R}^d$ denote the domain in the d-dimensional space, which is a bounded polygon (for $d = 2$) or polyhedron (for $d = 3$) with Lipschitz boundary $\partial\Omega$. The boundary is suitably decomposed into displacement and traction boundaries, $\partial\Omega_u$ and $\partial\Omega_t$, for the solid deformation problem, and pressure and flux boundaries, $\partial\Omega_p$ and $\partial\Omega_q$, for the fluid flow problem. The decomposed boundaries satisfy $\partial\Omega = \overline{\partial\Omega_u \cup \partial\Omega_t} = \overline{\partial\Omega_p \cup \partial\Omega_q}$ and $\varnothing = \partial\Omega_u \cap \partial\Omega_t = \partial\Omega_p \cap \partial\Omega_q$. The time interval of the problem is denoted by $\mathfrak{T} := (0, T]$ with $T > 0$.

The strong form of this problem is as follows. Given $\hat{\boldsymbol{u}}$, $\hat{\boldsymbol{t}}$, $\hat{p}$, $\hat{q}$, $\boldsymbol{u}_0$, and p_0, find $\boldsymbol{u}$ and p such that

$$\nabla \cdot (\boldsymbol{\sigma}'(\boldsymbol{u}) - S(p)p\mathbf{1}) + \rho\boldsymbol{g} = \mathbf{0} \quad \text{in} \quad \Omega \times \mathfrak{T}, \tag{9}$$

$$\phi\dot{S}(p) + S(p)\,\nabla \cdot \dot{\boldsymbol{u}} - \nabla \cdot (\boldsymbol{\kappa}(p) \cdot (\nabla p - \rho_w \boldsymbol{g})) = 0 \quad \text{in} \quad \Omega \times \mathfrak{T}, \tag{10}$$

subject to boundary conditions ($\boldsymbol{n}$ is the unit outward normal vector)

$$\boldsymbol{u} = \hat{\boldsymbol{u}} \quad \text{on} \quad \partial\Omega_u \times \mathfrak{T}, \tag{11}$$

$$\boldsymbol{n} \cdot \boldsymbol{\sigma}(\boldsymbol{u}) = \hat{\boldsymbol{t}} \quad \text{on} \quad \partial\Omega_t \times \mathfrak{T}, \tag{12}$$

$$p = \hat{p} \quad \text{on} \quad \partial\Omega_p \times \mathfrak{T}, \tag{13}$$

$$\boldsymbol{n} \cdot (\boldsymbol{\kappa}(p) \cdot (\nabla p - \rho_w \boldsymbol{g})) = \hat{q} \quad \text{on} \quad \partial\Omega_q \times \mathfrak{T}, \tag{14}$$

and initial conditions

$$\boldsymbol{u} = \boldsymbol{u}_0(\boldsymbol{x}), \quad p = p_0(\boldsymbol{x}), \tag{15}$$

for all position vectors $\boldsymbol{x} \in \Omega$ at time $t = 0$.

Remark 1. *Alternative formulations for poromechanics.* The foregoing two-field $\boldsymbol{u}/p$ formulation is perhaps the most widely used formulation for coupled poromechanics. Nevertheless, there exist several other types of poromechanical formulations in which different fields are primary variables (*e.g.*, [51–54, 69, 70]). A notable example is the three-field $\boldsymbol{u}/\boldsymbol{q}/p$ formulation, whereby lowest order Raviart–Thomas and piecewise constant spaces are used for the approximation of the seepage flux vector $\boldsymbol{q}$ and the pore pressure p, respectively. The three-field mixed formulation provides local mass conservation by construction. However, it also has a couple of potentially undesirable aspects. First, since the three-field formulation approximates the seepage flux vector as an additional field, it can be significantly more expensive than the two-field formulation especially for 3D problems. Second, the three-field formulation may not be well posed for undrained poromechanical problems because it uses the inverse of the permeability tensor in the governing equation. As such, it is still worthwhile to develop a locally mass conservative method for the two-field $\boldsymbol{u}/p$ formulation.

3. Numerical Methods

In this section, we develop a finite element formulation for the poromechanics problem that uses the EG method to discretize the mass balance equation in a locally conservative manner. We begin

this section with a description of the EG finite element method. We then apply the EG method to space discretization of the mass balance equation (2) in a locally conservative manner. For completeness, we then describe the space discretization of the momentum balance equation, the time discretization of the mass balance equation, and the fully discrete form of the poromechanical problem. Lastly, iterative solution strategies for the resulting discrete system are briefly discussed.

3.1. Enriched Galerkin finite element method

Let $\mathcal{T}_h$ be a shape-regular (*i.e.,* satisfying the minimum angle condition, see Ciarlet [71]) family of elements T partitioning Ω. We denote by h_T the diameter of T, and define $h := \max_{T\in\mathcal{T}_h} h_T$. Each element has edges (in 2D) or faces (in 3D) at its boundaries, which are commonly referred to as edges hereafter. Let $\mathcal{E}_h$ be the set of all element edges, which is decomposed into the set of internal edges $\mathcal{E}_h^\circ$ and the set of boundary edges $\mathcal{E}_h^\partial$. The set of boundary edges is further decomposed into $\mathcal{E}_h^\partial = \mathcal{E}_h^{\partial p} \cup \mathcal{E}_h^{\partial q}$, where $\mathcal{E}_h^{\partial p}$ is the set of edges at the Dirichlet type pressure boundary and $\mathcal{E}_h^{\partial q}$ is the set of edges at the Neumann type flux boundary.

The discrete space of the EG finite element approximation is set up as follows. First, we define the space of piecewise discontinuous polynomials of degree k as

$$\mathcal{V}_h^{\mathsf{DG}_k}(\mathcal{T}_h) := \{\psi \in L^2(\Omega) : \psi|_T \in \mathbb{Q}_k(T)\,,\ \forall\, T \in \mathcal{T}_h\}\,, \tag{16}$$

where $L^2(\Omega)$ is the space of square integrable functions and $\mathbb{Q}_k$ is the space of polynomials of degree at most k. For example, $\mathcal{V}_h^{\mathsf{DG}_0}(\mathcal{T}_h)$ is the space for piecewise constant approximation, and $\mathcal{V}_h^{\mathsf{DG}_1}(\mathcal{T}_h)$ is the space for the linear DG approximation. Next, let $V_h^{\mathsf{CG}_k}(\mathcal{T}_h)$ be the subspace of $\mathcal{V}_h^{\mathsf{DG}_k}(\mathcal{T}_h)$ consisting of piecewise continuous polynomials ($\mathbb{C}^0$), *i.e.,*

$$\mathcal{V}_h^{\mathsf{CG}_k}(\mathcal{T}_h) := \mathcal{V}_h^{\mathsf{DG}_k}(\mathcal{T}_h) \cap \mathbb{C}^0(\Omega)\,. \tag{17}$$

Accordingly, $\mathcal{V}_h^{\mathsf{CG}_k}(\mathcal{T}_h)$ is the space for the CG approximation with k-th degree polynomials. Then, the space for the EG discretization, $\mathcal{V}_h^{\mathsf{EG}_k}$, is defined as

$$\mathcal{V}_h^{\mathsf{EG}_k}(\mathcal{T}_h) := \mathcal{V}_h^{\mathsf{CG}_k}(\mathcal{T}_h) + \mathcal{V}_h^{\mathsf{DG}_0}(\mathcal{T}_h)\,. \tag{18}$$

In words, the EG space with k-th degree polynomials is constructed by adding (enriching) the piecewise constant functions to the CG finite element space. Figure 1 comparatively illustrates the degrees of freedom of the bilinear CG, DG, and EG methods for discretization of a 2D domain by four quadrilateral elements. It is noted that, for a sufficiently large number of elements, the degrees of the freedom for $\mathcal{V}_h^{\mathsf{EG}_1}(\mathcal{T}_h)$ are approximately 1/2 (in 2D) and 1/4 (in 3D) of the degrees of the freedom of $\mathcal{V}_h^{\mathsf{DG}_1}(\mathcal{T}_h)$. See [57, 58] for more details of the EG method including mathematical analyses.

In this work, we use weighted interior penalty methods (*e.g.,* [58, 72]) to construct the variational formulation of the mass balance equation. For this purpose, we define averages and jumps of scalar and vector functions on $\mathcal{E}_h$. For an interior edge $e \in \mathcal{E}_h^\circ$, we denote by T^+ and T^- the two elements sharing it, and by $\boldsymbol{n}^+$ and $\boldsymbol{n}^-$ their respective outward unit normals. Let ζ and $\boldsymbol{\tau}$ be a scalar field and a vector field, respectively, and $\zeta^\pm = \zeta|_{T^\pm}$ and $\boldsymbol{\tau}^\pm = \boldsymbol{\tau}|_{T^\pm}$. For $e \in \mathcal{E}_h^\circ$, we define the weighted

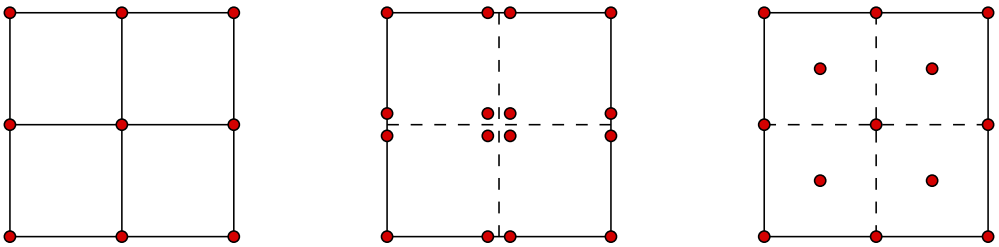

(a) CG-$\mathbb{Q}_1$ (b) DG-$\mathbb{Q}_1$ (c) EG-$\mathbb{Q}_1$

Figure 1: Comparison of the degrees of freedom for a 2D Cartesian grid ($\mathbb{Q}_1$) with linear CG, DG and EG approximations. In (c), the degrees of freedom in the middle of the elements indicate piecewise constant functions enriched to the finite element space of the CG method.

averages as

$$\{\zeta\}_{\delta_e} = \delta_e \zeta^+ + (1-\delta_e)\zeta^- \quad \text{and} \quad \{\boldsymbol{\tau}\}_{\delta_e} = \delta_e \boldsymbol{\tau}^+ + (1-\delta_e)\boldsymbol{\tau}^- , \tag{19}$$

where $\delta_e \in [0,1]$ is the weight. Next, we define the jumps as

$$[\![\zeta]\!] = \zeta^+ \boldsymbol{n}^+ + \zeta^- \boldsymbol{n}^- \quad \text{and} \quad [\![\boldsymbol{\tau}]\!] = \boldsymbol{\tau}^+ \cdot \boldsymbol{n}^+ + \boldsymbol{\tau}^- \cdot \boldsymbol{n}^- . \tag{20}$$

Note that the jump of a scalar quantity is a vector, whereas the jump of a vector quantity is a scalar. We also define the average and jump terms at the boundary as

$$[\![\zeta]\!] = \zeta \boldsymbol{n} \quad \text{and} \quad \{\boldsymbol{\tau}\}_{\delta_e} = \boldsymbol{\tau}, \quad \forall\, e \in \mathcal{E}_h^{\partial} . \tag{21}$$

The weight δ_e in the average operator $\{\cdot\}_{\delta_e}$ may be chosen at one's discretion. Here we adopt the choice of [60], given by

$$\delta_e = \beta_e := \frac{\kappa_e^-}{\kappa_e^+ + \kappa_e^-} , \tag{22}$$

where

$$\kappa_e^+ := (\boldsymbol{n}^+)^{\mathsf{T}} \cdot \boldsymbol{\kappa}^+ \cdot \boldsymbol{n}^+ \quad \text{and} \quad \kappa_e^- := (\boldsymbol{n}^+)^{\mathsf{T}} \cdot \boldsymbol{\kappa}^- \cdot \boldsymbol{n}^+ , \tag{23}$$

with $\boldsymbol{\kappa}^{\pm} := \boldsymbol{\kappa}|_{T^{\pm}}$. It is noted that the weight value varies over interior edges unless the permeability is homogeneous throughout the domain. We also define $\kappa_e = 2\kappa_e^+\kappa_e^-/(\kappa_e^+ + \kappa_e^+)$, *i.e.,* the harmonic mean of κ_e^+ and κ_e^-, and use it to scale interior penalty terms.

3.2. Space discretization of the mass balance equation

We now discretize the mass balance equation in space using the EG method. Let us denote the EG finite element space approximation of the pressure $p(\boldsymbol{x},t)$ by $p_h := p_h(\boldsymbol{x},t) \in V_h^{\mathsf{EG}_k}(\mathcal{T}_h)$. Since the saturation $S(\boldsymbol{x},t)$ and the lumped permeability tensor $\boldsymbol{\kappa}(\boldsymbol{x},t)$ are functions of pressure, we also denote their EG approximations by $S_h := S_h(\boldsymbol{x},t) \in V_h^{\mathsf{EG}_k}(\mathcal{T}_h)$ and $\boldsymbol{\kappa}_h := \boldsymbol{\kappa}_h(\cdot,t) \in V_h^{\mathsf{EG}_k}(\mathcal{T}_h)$, respectively. We assume that $\dot{\boldsymbol{u}}(\boldsymbol{x},t)$ is given for now. Denoting the variations of the trial pressure

solutions by $\psi \in \mathcal{V}_h^{\mathsf{EG}_k}(\mathcal{T}_h)$, the semi-discrete variational form of (10) is stated as

$$\begin{aligned}
&\sum_{T\in\mathcal{T}_h}\int_T \psi(\phi\dot{S}_h + S_h\,\nabla\cdot\dot{\boldsymbol{u}})\,\mathrm{d}V + \sum_{T\in\mathcal{T}_h}\int_T \nabla\psi\cdot\boldsymbol{\kappa}_h\cdot(\nabla p_h - \rho_w\boldsymbol{g})\,\mathrm{d}V\\
&-\sum_{e\in\mathcal{E}_h^\circ\cup\mathcal{E}_h^{\partial p}}\int_e [\![\psi]\!]\cdot\{\boldsymbol{\kappa}_h\cdot(\nabla p_h - \rho_w\boldsymbol{g})\}_{\delta_e}\,\mathrm{d}A\\
&+\sum_{e\in\mathcal{E}_h^\circ\cup\mathcal{E}_h^{\partial p}}\theta\int_e [\![p_h]\!]\cdot\{\boldsymbol{\kappa}_h\cdot\nabla\psi\}_{\delta_e}\,\mathrm{d}A + \sum_{e\in\mathcal{E}_h^\circ\cup\mathcal{E}_h^{\partial p}}\frac{\alpha}{h^e}\int_e \kappa_e\,[\![\psi]\!]\cdot[\![p_h]\!]\,\mathrm{d}A\\
&-\sum_{e\in\mathcal{E}_h^{\partial p}}\theta\int_e \hat{p}\boldsymbol{n}\cdot(\boldsymbol{\kappa}_h\cdot\nabla\psi)\,\mathrm{d}A - \sum_{e\in\mathcal{E}_h^{\partial p}}\frac{\alpha}{h^e}\int_e \kappa_e\,[\![\psi]\!]\cdot(\hat{p}\boldsymbol{n})\,\mathrm{d}A\\
&-\sum_{e\in\mathcal{E}_h^{\partial q}}\int_e \psi\hat{q}\,\mathrm{d}A = 0\,,\quad \forall\,\psi\in\mathcal{V}_h^{\mathsf{EG}_k}(\mathcal{T}_h)\,.
\end{aligned}\tag{24}$$

The use of interior penalty methods has introduced three new parameters in the above equation: (1) the edge length h^e, which is defined as $h^e := (\mathrm{meas}(T^+) + \mathrm{meas}(T^-))/2\,\mathrm{meas}(e)$, (2) the penalty parameter α, which is a function of the polynomial degree k, and (3) the penalty method parameter θ, which leads to the symmetric interior penalty Galerkin method (SIPG) when $\theta = -1$, the incomplete interior penalty Galerkin method (IIPG) [73, 74] when $\theta = 0$, and the non-symmetric interior penalty Galerkin method (NIPG) [75] when $\theta = 1$. In this work, we use the IIPG method.

Remark 2. *Conservation properties.* The discrete variational form (24) is both locally and globally conservative. To investigate the conservation properties, we define the discrete flux vector, $\boldsymbol{q}_h$, as

$$\boldsymbol{q}_h := -\boldsymbol{\kappa}_h\cdot(\nabla p_h - \rho_w\boldsymbol{g})\,,\quad \forall\,T\in\mathcal{T}_h\,,\tag{25}$$

$$\boldsymbol{q}_h\cdot\boldsymbol{n}^e := -\{\boldsymbol{\kappa}_h\cdot(\nabla p_h - \rho_w\boldsymbol{g})\cdot\boldsymbol{n}^e\} + (\alpha/h^e)[\![p_h]\!]\,,\quad \forall\,e\in\mathcal{E}_h^\circ\,,\tag{26}$$

$$\boldsymbol{q}_h\cdot\boldsymbol{n}^e := -\boldsymbol{\kappa}_h\cdot(\nabla p_h - \rho_w\boldsymbol{g})\cdot\boldsymbol{n}^e + (\alpha/h^e)(p_h - \hat{p})\,,\quad \forall\,e\in\mathcal{E}_h^{\partial p}\,,\tag{27}$$

$$\boldsymbol{q}_h\cdot\boldsymbol{n}^e := -\hat{q}\,,\quad \forall\,e\in\mathcal{E}_h^{\partial q}\,,\tag{28}$$

where $\boldsymbol{n}^e$ is the outward normal vector at the edge e. When e is a boundary edge, $\boldsymbol{n}^e$ coincide with the boundary normal vector $\boldsymbol{n}$. To extract the local mass conservation property, we set ψ as 1 in an element T and as 0 elsewhere. Then, (24) becomes

$$\int_T(\phi\dot{S}_h + S_h\,\nabla\cdot\dot{\boldsymbol{u}})\,\mathrm{d}V + \sum_{e\in\partial T}\int_e \boldsymbol{q}_h\cdot\boldsymbol{n}^e\,\mathrm{d}A = 0\,,\quad \forall\,T\in\mathcal{T}_h\,.\tag{29}$$

It is noted that CG discretization cannot attain this local conservation property since it does not allow ψ to be 1 exclusively inside an element. Another important characteristic that enables local mass conservation is the weak enforcement of Dirichlet boundary conditions. Moreover, to show that $\boldsymbol{q}_h$ is globally conservative, we take $\psi = 1$ throughout the domain and obtain

$$\int_\Omega(\phi\dot{S}_h + S_h\,\nabla\cdot\dot{\boldsymbol{u}})\,\mathrm{d}V + \int_{\partial\Omega}\boldsymbol{q}_h\cdot\boldsymbol{n}\,\mathrm{d}A = 0\,.\tag{30}$$

Therefore, the EG discretization provides mass conservation in the entire domain as well as every single element.

Remark 3. *DG discretization.* The variational form (24) can also be used for an interior penalty DG discretization of the same problem. The only change is that the solution and variation spaces become $\mathcal{V}_h^{\mathsf{DG}_k}(\mathcal{T}_h)$, instead of $\mathcal{V}_h^{\mathsf{EG}_k}(\mathcal{T}_h)$. As such, the EG and DG discretization methods have the same conservation properties.

Remark 4. *Penalty parameter.* The penalty parameter α in (24) comes from the weighted interior penalty method, and it has been studied extensively in the DG literature. In essence, the value of α controls the amount of inter-element continuity added to perfectly discontinuous elements. If α is too small, the discretized system would be unstable. Conversely, too large an α would enforce excessive inter-element continuity, rendering the discrete system very close to that from the CG discretization of the same problem. In our numerical results, $\alpha \approx 100$ is a good choice. Readers interested in this aspect are referred to [76–78] and references therein.

Remark 5. *Decomposition into CG and piecewise constant DG parts.* As shown in (18), the EG space is constructed by addition of the CG space and the piecewise constant DG space. Accordingly, the trial solutions and variations discretized by the EG method, $p_h \in \mathcal{V}_h^{\mathsf{EG}_k}(\mathcal{T}_h)$ and $\psi \in \mathcal{V}_h^{\mathsf{EG}_k}(\mathcal{T}_h)$, respectively, are additively decomposed as

$$p_h = p_h^{\mathsf{CG}_k} + p_h^{\mathsf{DG}_0} \quad \text{and} \quad \psi = \psi^{\mathsf{CG}_k} + \psi^{\mathsf{DG}_0}, \tag{31}$$

where $p_h^{\mathsf{CG}_k}, \psi^{\mathsf{CG}_k} \in \mathcal{V}_h^{\mathsf{CG}_k}(\mathcal{T}_h)$ and $p_h^{\mathsf{DG}_0}, \psi^{\mathsf{DG}_0} \in \mathcal{V}_h^{\mathsf{DG}_0}(\mathcal{T}_h)$. Inserting (31) into (24), one can identify terms that are augmented to the standard CG formulation. It should be noted that many of these new terms indeed vanish due to the characteristics of piecewise continuous polynomials $(\cdot)^{\mathsf{CG}_k}$ and piecewise constants $(\cdot)^{\mathsf{DG}_0}$. Specifically, since continuous polynomials do not have jump across edges, $[\![\psi^{\mathsf{CG}_k}]\!] = [\![p^{\mathsf{CG}_k}]\!] = 0$, and since ψ^{DG_0} and p^{DG_0} are constant in each element, $\nabla \psi^{\mathsf{DG}_0} = \nabla p^{\mathsf{DG}_0} = 0$. Canceling these terms out remarkably simplifies the variational formulation. It is also noted that $\nabla \psi \neq 0$ since $\nabla \psi^{\mathsf{CG}_k} \neq 0$.

Remark 6. *Number of unknowns.* Detailed comparisons of the number of unknowns for CG, DG, and EG methods are presented in [57, 58] for both a structured rectangular mesh and an unstructured triangles/tetrahedra mesh in 2D and 3D. For example, for a given $N \times N$ 2D rectangular mesh, the number of unknowns for linear CG, DG, and EG are $(N+1)^2$, $4N^2$, and $(2N+1)^2$, respectively. When the mesh size (h) and polynomial order (p) are identical, the three methods have the same optimal order of error convergence, although their specific errors may vary. Since our focus is local mass conservation, the proposed EG formulation will be compared with the CG formulation which is widely used for poromechanics and does not provide local mass conservation. The comparison will be made for fixed h and p, because local mass conservation in poromechanics is particularly motivated for heterogeneous problems of which spatial discretization is likely to be governed by the length scale of heterogeneity. For homogeneous problems, it may be advantageous to use larger elements with higher-order approximations to get a numerical solution of similar accuracy. Note, however, that other factors such as iterative solvers and the number of Gauss points (for plasticity problems) also determine the overall computational cost. As always, the selection of an optimal numerical method does not have a definite answer and it is at the discretion of the numerical analyst.

The primary purpose of this work is to introduce EG as a local mass conservative method involving fewer unknowns than DG for the same h and p.

3.3. Space discretization of the linear momentum balance equation

As for discretization of the balance of linear momentum equation (9), we use the CG method since it is good enough for the deformation problems of our interests. For the CG discretization, we define the finite element spaces for using continuous piecewise polynomials:

$$\mathcal{W}_h^{\mathsf{CG}_k}(\mathcal{T}_h) := \{\boldsymbol{\eta} \in \mathbb{C}^0(\Omega) : \boldsymbol{\eta}|_T \in \mathbb{Q}_k(T)\,,\ \forall\, T \in \mathcal{T}_h\}\,, \tag{32}$$

$$\bar{\mathcal{W}}_h^{\mathsf{CG}_k}(\mathcal{T}_h) := \{\boldsymbol{\eta} \in \mathbb{C}^0(\Omega) : \boldsymbol{\eta} = \mathbf{0}\,, \boldsymbol{\eta}|_T \in \mathbb{Q}_k(T)\,,\ \forall\, T \in \mathcal{T}_h\}\,. \tag{33}$$

Let us denote the CG finite element space approximation of the displacement vector $\boldsymbol{u}(\boldsymbol{x}, t)$ by $\boldsymbol{u}_h := \boldsymbol{u}_h(\boldsymbol{x}, t) \in \mathcal{W}_h^{\mathsf{CG}_k}(\mathcal{T}_h)$. Accordingly, the discretized effective stress tensor is denoted by $\boldsymbol{\sigma}'_h$. Following the standard procedure, we can express the discrete variational form of the balance of linear momentum as

$$\begin{aligned} &-\int_\Omega \nabla^{\mathrm{s}}\boldsymbol{\eta} : \boldsymbol{\sigma}'_h \,\mathrm{d}V + \int_\Omega S_h p_h \nabla\cdot\boldsymbol{\eta}\,\mathrm{d}V \\ &+\int_\Omega \boldsymbol{\eta}\cdot\rho\boldsymbol{g}\,\mathrm{d}V + \int_{\partial\Omega_t}\boldsymbol{\eta}\cdot\hat{\boldsymbol{t}}\,\mathrm{d}A = 0\,, \quad \forall\,\boldsymbol{\eta} \in \bar{\mathcal{W}}_h^{\mathsf{CG}_k}(\mathcal{T}_h)\,. \end{aligned} \tag{34}$$

The rest of the CG discretization procedure is straightforward, and its details can be found in [79] and many others.

Remark 7. *Inf–sup stability.* It is well known that mixed finite elements for coupled poromechanics are subject to an inf–sup stability condition in the limit of undrained deformation [19, 27, 31, 32]. This is because, during undrained deformation, the pore pressure acts as an incompressibility constraint, rendering the discrete system a saddle point problem much like that of mixed finite elements for Stokes problems. Notably, Taylor–Hood elements [80] have been proven to satisfy the inf–sup condition of mixed CG/EG elements for velocity/pressure discretization of Stokes flow problems [81]. On the other hand, when the fluid flow is compressible (*e.g.,* in the drained or unsaturated condition), the discrete problem does not have a saddle point structure and so the mixed finite elements are not restricted by a stability condition. In such cases, equal-order elements may be an efficient choice for obtaining a pressure solution of the same order of accuracy. Therefore, in this work we use Taylor–Hood elements when the problem of interest involves undrained deformation, and use equal-order elements when it does not.

3.4. Time discretization of the mass balance equation

The variational mass balance equation (24) contains the time derivatives of $\boldsymbol{u}_h$ (after the CG discretization as described above) and S_h. To discretize these variables in time, we use the implicit Euler method. For a given time increment $\Delta t := t^{n+1} - t^n$ from time t^n to t^{n+1}, the time derivatives of these variables are approximated as

$$\dot{\boldsymbol{u}}_h = \frac{\boldsymbol{u}_h^{n+1} - \boldsymbol{u}_h^n}{\Delta t} \quad \text{and} \quad \dot{S}_h = \frac{S_h^{n+1} - S_h^n}{\Delta t}\,, \tag{35}$$

where $(\cdot)^{n+1}$ and $(\cdot)^n$ denote the quantities at time t^{n+1} and t^n, respectively. It is noted that the saturation variable is discretized directly, not after being expanded by the chain rule as $\dot{S} = S'(p)\dot{p}$. This is because the use of $S'(p)$ in a time-discrete setting can lead to large mass balance errors, see Celia *et al.* [82]. We complete the time discretization by inserting (35) into (24), and evaluate all other variables in (24) and (34) at time t^{n+1}. We also multiply the discrete mass balance equation by Δt, as common in the discretization of poromechanical formulations (*e.g.,* [27, 32]).

3.5. *Fully discrete form of the poromechanical formulation*

Now we write the fully discrete form of the poromechanical problem. Let $\hat{\boldsymbol{u}}^{n+1}$, $\hat{\boldsymbol{t}}^{n+1}$, $\hat{p}^{n+1}$, and $\hat{q}^{n+1}$ be approximations of $\hat{\boldsymbol{u}}(\boldsymbol{x}, t^{n+1})$, $\hat{\boldsymbol{t}}(\boldsymbol{x}, t^{n+1})$, $\hat{p}(\boldsymbol{x}, t^{n+1})$, and $\hat{q}(\boldsymbol{x}, t^{n+1})$, respectively. We also set the initial condition for the pressure as $p_h^0 := \Pi_h^{\mathsf{EG}}\, p(\boldsymbol{x}, 0)$, where Π_h^{EG} is the interpolation operator for the EG space $\mathcal{V}_h^{\mathsf{EG}_k}(\mathcal{T}_h)$ [58]. Then the discrete problem reads as follows: Given $\boldsymbol{u}_h^n$ and p_h^n, find $(\boldsymbol{u}_h^{n+1}, p_h^{n+1}) \in \mathcal{W}_h^{\mathsf{CG}_k}(\mathcal{T}_h) \times \mathcal{V}_h^{\mathsf{EG}_k}(\mathcal{T}_h)$ such that

$$\mathcal{A}(\boldsymbol{u}_h^{n+1}, p_h^{n+1}; \boldsymbol{\eta}, \psi) = \mathcal{F}(\boldsymbol{\eta}, \psi)\,, \quad \forall\, (\boldsymbol{\eta}, \psi) \in \bar{\mathcal{W}}_h^{\mathsf{CG}_k}(\mathcal{T}_h) \times \mathcal{V}_h^{\mathsf{EG}}(\mathcal{T}_h)\,, \tag{36}$$

where $\mathcal{A}$ is the bilinear form, defined as

$$\mathcal{A}(\boldsymbol{u}_h^{n+1}, p_h^{n+1}; \boldsymbol{\eta}, \psi) := a(\boldsymbol{u}_h^{n+1}, \boldsymbol{\eta}) + b(p_h^{n+1}, \boldsymbol{\eta}) + c(\boldsymbol{u}_h^{n+1}, \psi) + d(p_h^{n+1}, \psi)\,, \tag{37}$$

with

$$a(\boldsymbol{u}_h^{n+1}, \boldsymbol{\eta}) := -\int_\Omega \nabla^{\mathrm{s}} \boldsymbol{\eta} : \boldsymbol{\sigma}_h'^{n+1}\, \mathrm{d}V\,, \tag{38}$$

$$b(p_h^{n+1}, \boldsymbol{\eta}) := \int_\Omega S_h^{n+1} p_h^{n+1} \nabla \cdot \boldsymbol{\eta}\, \mathrm{d}V\,, \tag{39}$$

$$c(\boldsymbol{u}_h^{n+1}, \psi) := \sum_{T \in \mathcal{T}_h} \int_T \psi S_h^{n+1} \nabla \cdot (\boldsymbol{u}_h^{n+1} - \boldsymbol{u}_h^n)\, \mathrm{d}V\,, \tag{40}$$

$$\begin{aligned} d(p_h^{n+1}, \psi) := {} & \sum_{T \in \mathcal{T}_h} \int_T \psi \phi (S_h^{n+1} - S_h^n)\, \mathrm{d}V + \sum_{T \in \mathcal{T}_h} \Delta t \int_T \nabla \psi \cdot \boldsymbol{\kappa}_h^{n+1} \cdot (\nabla p_h^{n+1} - \rho \boldsymbol{g})\, \mathrm{d}V \\ & - \sum_{e \in \mathcal{E}_h^\circ \cup \mathcal{E}_h^{\partial p}} \Delta t \int_e [\![\psi]\!] \cdot \{\boldsymbol{\kappa}_h^{n+1} \cdot (\nabla p_h^{n+1} - \rho \boldsymbol{g})\}_{\delta_e}\, \mathrm{d}A \\ & + \sum_{e \in \mathcal{E}_h^\circ \cup \mathcal{E}_h^{\partial p}} \Delta t\, \theta \int_e [\![p_h^{n+1}]\!] \cdot \{\boldsymbol{\kappa}_h^{n+1} \cdot \nabla \psi\}_{\delta_e}\, \mathrm{d}A \\ & + \sum_{e \in \mathcal{E}_h^\circ \cup \mathcal{E}_h^{\partial p}} \Delta t\, \frac{\alpha}{h^e} \int_e \kappa_e\, [\![\psi]\!] \cdot [\![p_h^{n+1}]\!]\, \mathrm{d}A\,, \end{aligned} \tag{41}$$

and $\mathcal{F}$ is the linear functional, defined as

$$\mathcal{F}(\boldsymbol{\eta}, \psi) := f(\boldsymbol{\eta}) + g(\psi)\,, \tag{42}$$

with

$$f(\boldsymbol{\eta}) := -\int_{\Omega} \boldsymbol{\eta} \cdot \rho \boldsymbol{g} \, \mathrm{d}V - \int_{\partial\Omega_t} \boldsymbol{\eta} \cdot \hat{\boldsymbol{t}}^{n+1} \, \mathrm{d}A \tag{43}$$

$$\begin{aligned} g(\psi) := & \sum_{e \in \mathcal{E}_h^{\partial p}} \Delta t \, \theta \int_e \hat{p}^{n+1} \boldsymbol{n} \cdot (\boldsymbol{\kappa}_h^{n+1} \cdot \nabla \psi) \, \mathrm{d}A \\ & + \sum_{e \in \mathcal{E}_h^{\partial p}} \Delta t \, \frac{\alpha}{h^e} \int_e \kappa_e \, [\![\psi]\!] \cdot (\hat{p}^{n+1} \boldsymbol{n}) \, \mathrm{d}A \\ & + \sum_{e \in \mathcal{E}_h^{\partial q}} \Delta t \int_e \psi \hat{q}^{n+1} \, \mathrm{d}A \, . \end{aligned} \tag{44}$$

3.6. Solution strategy

To solve the discrete problem (36), we use Newton's method since the problem is nonlinear unless the material is fully saturated and linear elastic. In each Newton iteration, one must solve the following Jacobian system that emanates from the linearization of (36):

$$\begin{bmatrix} J_{uu} & J_{up} \\ J_{pu} & J_{pp} \end{bmatrix} \begin{Bmatrix} \delta \boldsymbol{u}_h \\ \delta p_h \end{Bmatrix} = - \begin{Bmatrix} R_u \\ R_p \end{Bmatrix} . \tag{45}$$

Here, $\delta \boldsymbol{u}_h$ and δp_h denote Newton increments of the displacement and the pressure unknowns, respectively. The residual vectors on the right hand side are defined as

$$R_u := a(\boldsymbol{u}_h^{n+1}, \boldsymbol{\eta}) + b(p_h^{n+1}, \boldsymbol{\eta}) \, , \tag{46}$$

$$R_p := c(\boldsymbol{u}_h^{n+1}, \psi) + d(p_h^{n+1}, \psi) \, . \tag{47}$$

Accordingly, the sub-matrices of the Jacobian matrix are given by

$$J_{uu} := \frac{\partial a(\boldsymbol{u}_h^{n+1}, \boldsymbol{\eta})}{\partial \boldsymbol{u}_h^{n+1}} \, , \quad J_{up} := \frac{\partial b(p_h^{n+1}, \boldsymbol{\eta})}{\partial p_h^{n+1}} \, , \quad J_{pu} := \frac{\partial c(\boldsymbol{u}_h^{n+1}, \psi)}{\partial \boldsymbol{u}_h^{n+1}} \, , \quad J_{pp} := \frac{\partial d(p_h^{n+1}, \psi)}{\partial p_h^{n+1}} \, . \tag{48}$$

The closed forms of these sub-matrices are obtained through a straightforward extension of those in CG formulations (see [28, 34] for example). The exact Jacobian matrix is used in this work.

However, efficient solution of this linear system is a significant challenge, which still remains an active area of research. Broadly speaking, strategies for fully coupled numerical solution of discrete poromechanical problems can be categorized into two classes: (1) monolithic methods which solve the solid deformation and fluid flow problems simultaneously, and (2) sequential methods which solve either the deformation or the flow problem until the coupled solution converges. The sequential methods allow for efficient combination of separate computer programs originally developed for either the fluid flow or the solid deformation problem, with a good convergence behavior when an appropriate split method is employed [48, 83]. However, as shown by White *et al.* [36], when proper preconditioning is used, a monolithic method has superior performance to a sequential method. Here we use the block-preconditioned monolithic method described in [28, 36], which

solves the linear system via two sequential steps of preconditioned Krylov iterations with multigrid preconditioners. The tolerances for both the Newton and Krylov iterations are set as 10^{-9}.

We also note that the block-preconditioning approach may be extended further to solve the EG-discretized pressure system more efficiently. The reason is that the pressure block can also have a nested 2 by 2 block structure owing to the decomposition of the EG space into the CG space and the piecewise constant DG space, namely $p_h = p_h^{\mathrm{CG}_k} + p_h^{\mathrm{DG}_0}$. In this case, the Jacobian system (45) can be expanded to

$$\begin{bmatrix} J_{uu} & J_{up}^{\mathrm{CG}_k} & J_{up}^{\mathrm{DG}_0} \\ J_{pu}^{\mathrm{CG}_k} & J_{pp}^{\mathrm{CG}_k/\mathrm{DG}_0} & J_{pp}^{\mathrm{DG}_0/\mathrm{CG}_k} \\ J_{pu}^{\mathrm{DG}_0} & J_{pp}^{\mathrm{DG}_0/\mathrm{CG}_k} & J_{pp}^{\mathrm{DG}_0/\mathrm{DG}_0} \end{bmatrix} \begin{Bmatrix} \delta \boldsymbol{u}_h \\ \delta p_h^{\mathrm{CG}_k} \\ \delta p_h^{\mathrm{DG}_0} \end{Bmatrix} = - \begin{Bmatrix} R_u \\ R_p^{\mathrm{CG}_k} \\ R_p^{\mathrm{DG}_0} \end{Bmatrix}, \tag{49}$$

as if $p_h^{\mathrm{CG}_k}$ and $p_h^{\mathrm{DG}_0}$ were distinct field variables in the formulation. Indeed, exploiting such a block structure in EG discretization, Lee *et al.* [58] have proposed efficient iterative solvers for EG methods for flow and transport in porous media. We believe that the same approach can be cast into block-partitioned solvers for poromechanics. For now, we leave this extension as a future research topic, and use the existing poromechanics solver.

4. Numerical Examples

Three numerical examples are presented in this section to study the accuracy and performance of the proposed numerical method. The first example verifies the numerical method using a well-known benchmark problem in poromechanics. The second and third examples demonstrate the performance and robustness of the proposed EG method in comparison with the classical CG method. In these examples, while the pressure field is approximated by different methods, the displacement field is commonly approximated by the CG method. Therefore, for brevity, we shall simply mention the numerical method for the pressure field approximation when comparing the results of different numerical methods. For example, the mixed CG/EG discretization of the displacement/pressure fields will be referred to as "EG."

The numerical examples are performed using `Geocentric`, a massively parallel finite element code for geomechanics built upon the `deal.II` finite element library [84, 85], `p4est` mesh handling library [86], and the `Trilinos` project [87].

4.1. Terzaghi's 1D consolidation problem

To verify the numerical formulation and its implementation, we first consider the analytical solutions for the classical Terzaghi's 1D consolidation problem. Figure 2 illustrates the setup of this problem. The material is homogeneous, linear elastic, isotropic, and fully saturated throughout the consolidation process. To express the analytical solution for pore pressure, we define the following non-dimensional quantities:

$$p^* = \frac{p}{w}, \quad z^* = \frac{z}{H}, \quad t^* = \left(\frac{c_v}{H^2}\right) t. \tag{50}$$

Here, p is the pore pressure, w is the distributed load at the drainage boundary, z is the distance from the drainage boundary, H is the domain thickness, t is time, and c_v is the coefficient of consolidation. One can express c_v in terms of the bulk modulus K, Poisson's ratio ν, the isotropic permeability k_i, and the fluid dynamic viscosity μ, as

$$c_v = 3K\left(\frac{1-\nu}{1+\nu}\right)\frac{k_i}{\mu}\,. \tag{51}$$

Then the analytical solution for pressure can be written as

$$p^*(z^*, t^*) = \sum_{m=0}^{\infty} \frac{2}{M}\sin(Mz^*)e^{-M^2 t^*}\,, \quad M = \pi(2m+1)/2\,. \tag{52}$$

For this specific example, we assign $H = 1$ m, $w = 1$ kPa, the isotropic permeability $k_i = 10^{-12}$ m^2, the dynamic viscosity $\mu = 10^{-6}$ kPa·s, the bulk modulus of 1000 kPa, and Poisson's ratio of 0.25. These values give the coefficient of consolidation $c_v = 0.0018$ m^2/s.

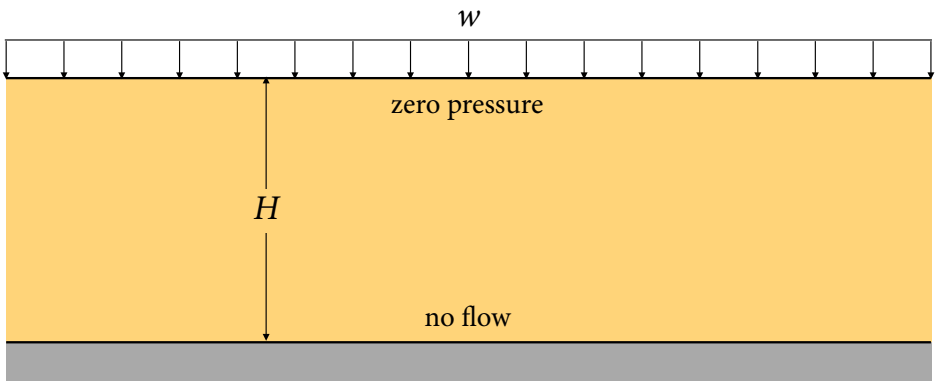

Figure 2: Setup of the 1D consolidation problem.

Using this analytical solution for the consolidation problem, we examine whether the proposed EG formulation manifests the expected convergence rates upon mesh refinement. For this purpose, we first solve this problem using the proposed EG method, with $h = 0.1$ m (10 uniform quadrilateral elements) and $\Delta t = 0.01t^*$ s. The EG solutions of the pore pressure fields at $t^* = 0.05$, 0.1, 0.25, and 0.5 are presented in Fig. 3 along with the corresponding analytical solutions.

We then perform an error convergence test with respect to the analytical solution (52) at $t^* = 0.1$. For comparison, we also conduct the same convergence test with the classical CG method. Both of the EG and CG methods use bilinear basis functions ($\mathbb{Q}_1$) for the mass balance equation, whereas they discretize the momentum balance equation by CG-$\mathbb{Q}_2$ elements (*i.e.,* Taylor–Hood elements) since several initial steps may involve undrained conditions. For each of the errors $p - p_h$ of the EG and CG solutions, we compute the $L^2(\Omega)$-norm $\|p - p_h\|_{L^2(\Omega)}$ and the $H^1(\Omega)$-seminorm $|p - p_h|_{H^1(\Omega)}$. To isolate the spatial errors, we reduce the time step size by 1/4 while reducing the mesh size by 1/2.

Table 1 shows the $L^2(\Omega)$-norm and $H^1(\Omega)$-seminorm errors of the numerical solutions with respect to the mesh size. The expected optimal order of convergences are observed for both EG and

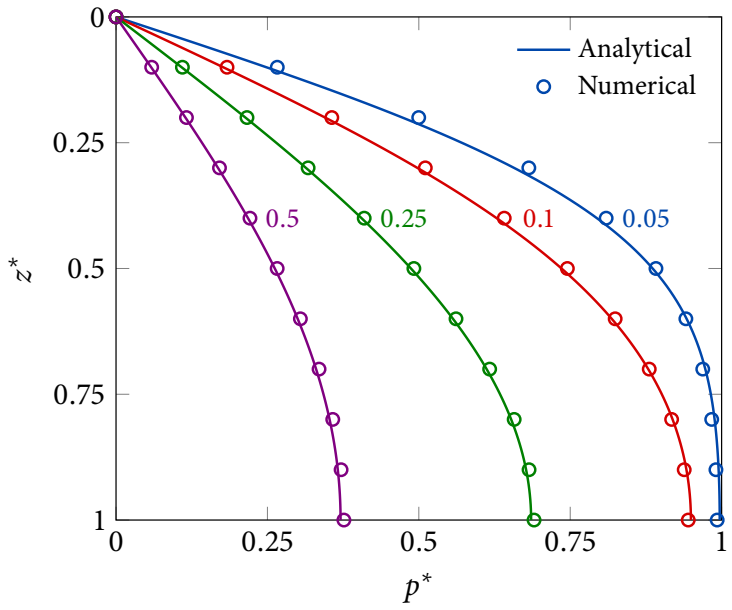

Figure 3: Analytical solutions for pressure in the 1D consolidation problem and their numerical approximations by EG-$\mathbb{Q}_1$ with $h = 0.1$ m and $\Delta t = 0.01t^*$ s. Numbers next to the lines denote t^*.

CG solutions (*i.e.,* 2 in the L^2-norm and 1 in the H^1-seminorm). The results confirm that the EG method also provides optimal solutions when the CG method does. We refer to Lee *et al.* [58] for the analysis of EG methods for general elliptic and parabolic equations.

	EG				CG			
h_0/h	L^2 error	Rate	H^1 error	Rate	L^2 error	Rate	H^1 error	Rate
1	2.18e-03	-	2.04e-02	-	2.15e-03	-	2.04e-02	-
2	5.56e-04	2.0	9.02e-03	1.2	5.49e-04	2.0	9.02e-03	1.2
4	1.40e-04	2.0	4.35e-03	1.1	1.38e-04	2.0	4.35e-03	1.1
8	3.50e-05	2.0	2.15e-03	1.0	3.45e-05	2.0	2.15e-03	1.0

Table 1: Convergence test results of the 1D consolidation problem with the EG and CG methods.

4.2. 1D consolidation of a two-layered material

The purpose of the second example is to concisely demonstrate how the EG method can be advantageous for a coupled poromechanical problem whereby the pore pressure field manifests a shock-like change. For this purpose, we extend the previous example to involve a discontinuous permeability at the center of the domain, by setting $k_i = 10^{-16}$ m^2 at the lower half of the domain which is 10^{-4} times lower than the permeability of the upper half. It is noted that such a permeability jump is common in subsurface systems due to layers and other reasons; however, it often results in nonphysical pressure oscillations in CG solutions.

For comparison purposes, we solve this layered consolidation problem with both the EG and CG discretization methods. Again, for the inf–sup stability, we use $\mathbb{Q}_1$ elements for the pore pressure interpolation and $\mathbb{Q}_2$ elements for the solid displacement interpolation. We consider two levels of mesh sizes, $h = 0.025$ m and $h = 0.0125$ m (corresponding to $h_0/h = 4$ and 8 in the previous example), and set $\Delta t = 1$ s for both cases. Other physical and numerical properties remain the same from the previous example.

Figure 4 shows the pore pressure solutions at four time instances ($t = 25$, 50, 100, and 200 seconds) obtained by the EG and CG pressure approximations with the two mesh sizes. One can see that all the CG pressure solutions exhibit nonphysical oscillations at the top of the low-permeability layer (right below 0.5 m). Such oscillations are commonly observed from CG solutions of poromechanics near a discontinuous permeability region or a drainage boundary (see Fig. 5 of White and Borja [27] for example), and they are owing to the continuity enforcement of CG discretization. These spurious oscillations are somewhat alleviated by mesh refinement, but not sufficiently. Indeed, removal of this type of numerical oscillation in a CG solution usually requires a very fine discretization.

In contrast, every EG solution in Fig. 4 captures the sharp change in the pressure field without any non-physical oscillation, irrespective of the mesh size and the time instance. This achievement is thanks to the piecewise constant basis functions enriched to the CG space, which allow the overall solution to be nonconforming. It is noted that the decreasing pore pressure below the layer interface is due to the physical diffusion of pore pressure during the consolidation of the lower layer. The added number of the degrees of freedom is just the number of elements in each case: 40 in the $h = 0.025$ m case and 80 in the $h = 0.0125$ m case. Therefore, this example demonstrates how the EG method enables us to solve challenging yet realistic poromechanical problems with minimal additional costs to the CG method.

4.3. Unsaturated flow in a vertical cut with random permeability

Lastly, we consider a more complex problem that involves unsaturated flow in heterogeneous media. We particularly simulate the problem of wetting collapse of an unsaturated soil with random permeability. Figure 5 depicts the setup of this problem. The domain is a 15 m long and 5 m high rectangle, and its log permeability field is generated using an exponential covariance model as shown in the figure. The bottom and the right side of the domain are supported by pins and rollers, respectively, whereas the top and the left side are unsupported. Such an unsupported vertical cut is possible on unsaturated soil due to the presence of capillary forces. However, when this soil is continuously infiltrated by water, it progressively loses the capillary forces and collapses ultimately. To simulate this wetting collapse process, we apply a constant flux of 30 mm/h on the top of the domain, and assign no flux boundary conditions elsewhere. The initial capillary pressure is 25 kPa throughout the domain. 18 The soil domain is modeled as an elastoplastic material to simulate the onset of the collapse. We specifically use a perfectly plastic Drucker–Prager model [88], which is suitable for modeling shear failure of a pressure-sensitive material [66, 67, 89]. The material parameters of this model are: the cohesion of 5 kPa, the friction angle of 28°, and the dilation angle of 5°. In addition, to efficiently deal with the cone of the Drucker–Prager surface, we employ a hyperbolic approximation of the surface with the shape parameter of 0.1 (see [90, 91] for more details of this approximation). The elastic response is considered linear elastic with the bulk modulus of 5000

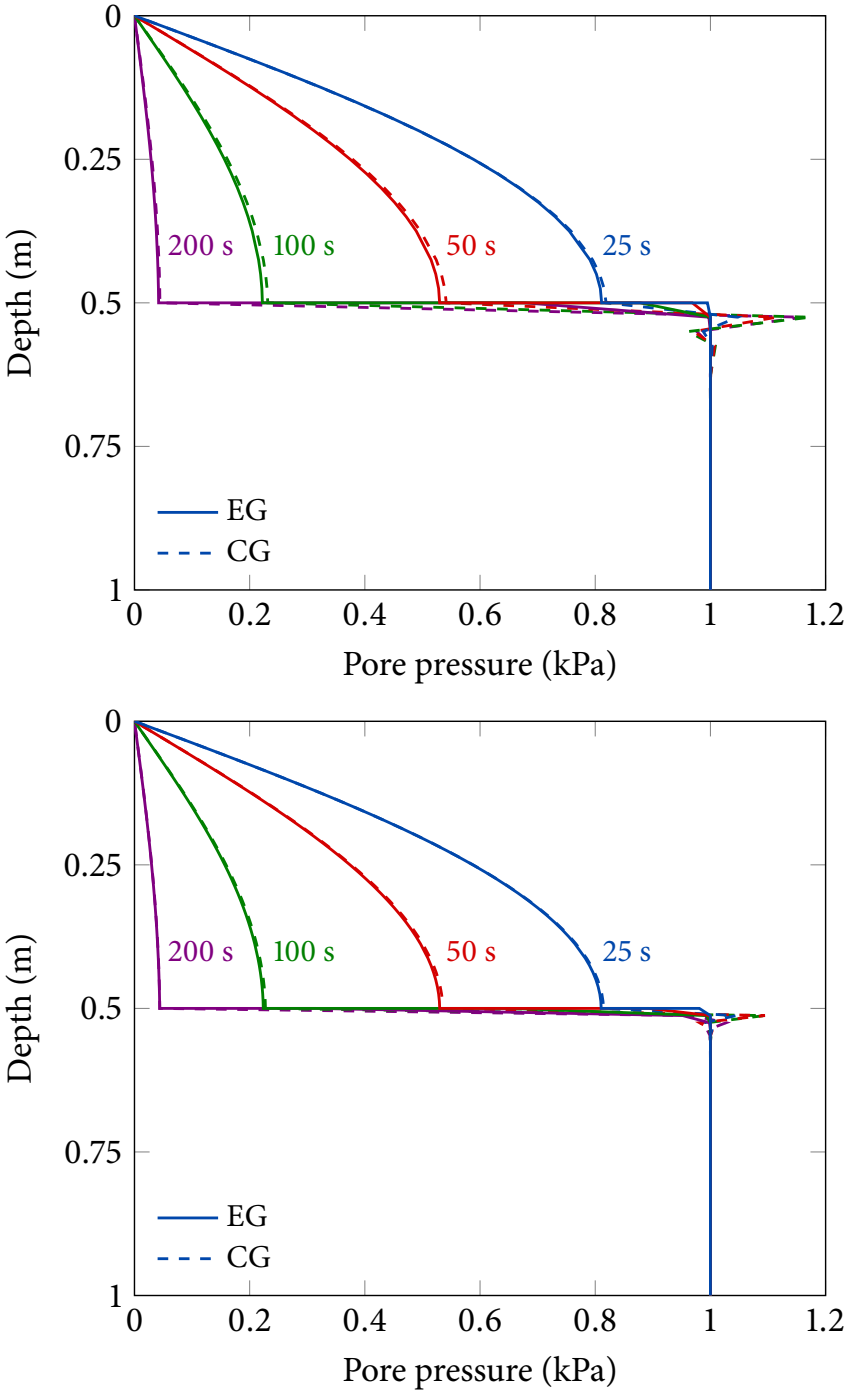

Figure 4: Pore pressure solutions of the layered consolidation problem obtained by EG and CG methods. (a) $h = 0.025$ m and (b) $h = 0.0125$ m.

Figure : Setup of the unsaturated žow problem. Illustrated inside the domain is the log permeability •eld.

kPa and Poisson's ratio of ý.ç. As for the non-deformation responses, we assign the van Genuchten parameters $S_{\hat{O}}$ ý.ç, $S_{\grave{o}}$ Ô.ýs Ô kPa, and d ç.ý; the intrinsic densities $_s$ ò.ý t/m^{ç} and $-_w$ Ô.ý t/m^{ê}; the porosity $^{\wedge}$ ý. ; and the dynamic viscosity $¼_w$ Ôý^{â} kPas.

e numerical simulation proceeds as follows. Once we discretize the domain by Ôòýý elements as shown in Fig. , we approximate the mass balance equation with two dišerent methods: one by EG-$Q_{\hat{O}}$ with ò¥—Ô pressure degrees of freedom and the other by CG-$Q_{\hat{O}}$ with Ôò—Ô pressure degrees of freedom. e momentum balance equation is approximated by CG-$Q_{\hat{O}}$ with ò âò displacement degrees of freedom. Note that this equal-order interpolation does not encounter a stability issue since this problem does not involve an undrained condition.en, we run gravity loading steps without boundary žuxes, until the domain reaches mechanical and hydraulic equilibrium.ese gravity loading steps are essential because not only the plasticity model depends on the con•ning pressure but also the initially uniform capillary pressure is not under equilibrium due to the heterogeneous permeability •eld. Subsequently, we begin the in•ltration process by applying the boundary žuxes, and proceed the simulation with the time step size Δt Ô minute. e simulation is halted when a signi•cant plastic strain (say, a zone of ò±ç percents of equivalent plastic strain) has developed, which may be thought as the onset of wetting collapse. It is noted that deformation beyond this point is inherently large and rapid, which is inappropriate to be modeled by the current in•nitesimal and quasi-static formulation. Lastly, as in the previous examples, we repeat the simulation with the CG method.

Figure â presents the pore pressure •elds of the EG solutions aŸer ¥ýý, —ýý, and Ôòýý minutes of water in•ltration. Due to the in•ltration from the top boundary, the pore pressure increases from the upper part of the domain. e wetting front is far from being straight as a consequence of the strong heterogeneity in the permeability •eld. It is noted that not only the absolute permeability •eld of this domain is heterogeneous as depicted in Fig. , but the relative permeability •eld also evolves heterogeneously by saturation changes during the in•ltration process. Due to this strong heterogeneity in both the absolute and relative permeability •elds, the leŸ side of the wetting front reaches the bottom of the domain earlier than other parts.

Figure À: Log of the residual norm of the local mass balance (ç) of the EG solutions aŸer ¥ýý, —ýý, and Ôòýý minutes.

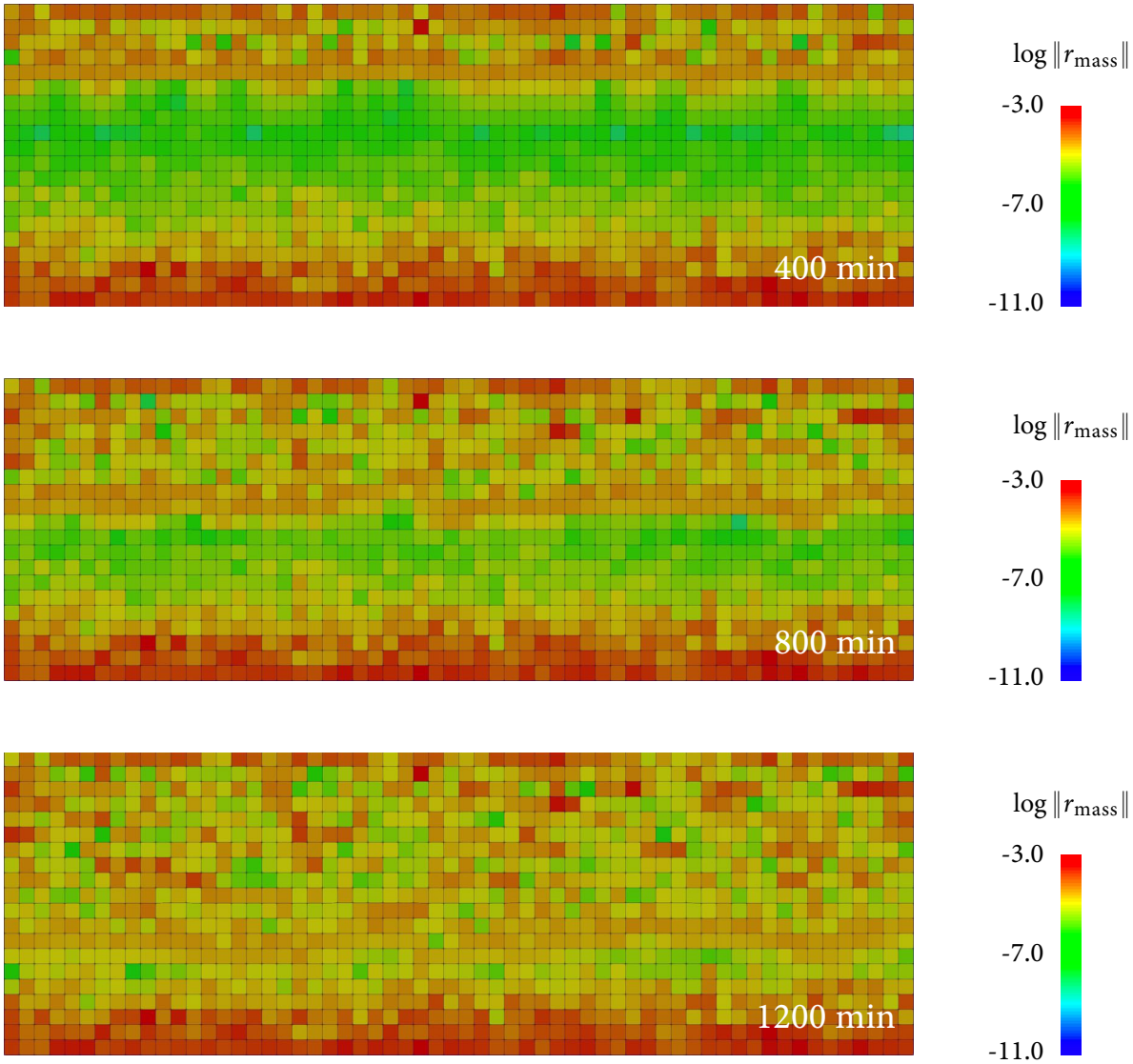

Figure 10: Log of the residual norm of the local mass balance (53) of the CG solutions after 400, 800, and 1200 minutes.

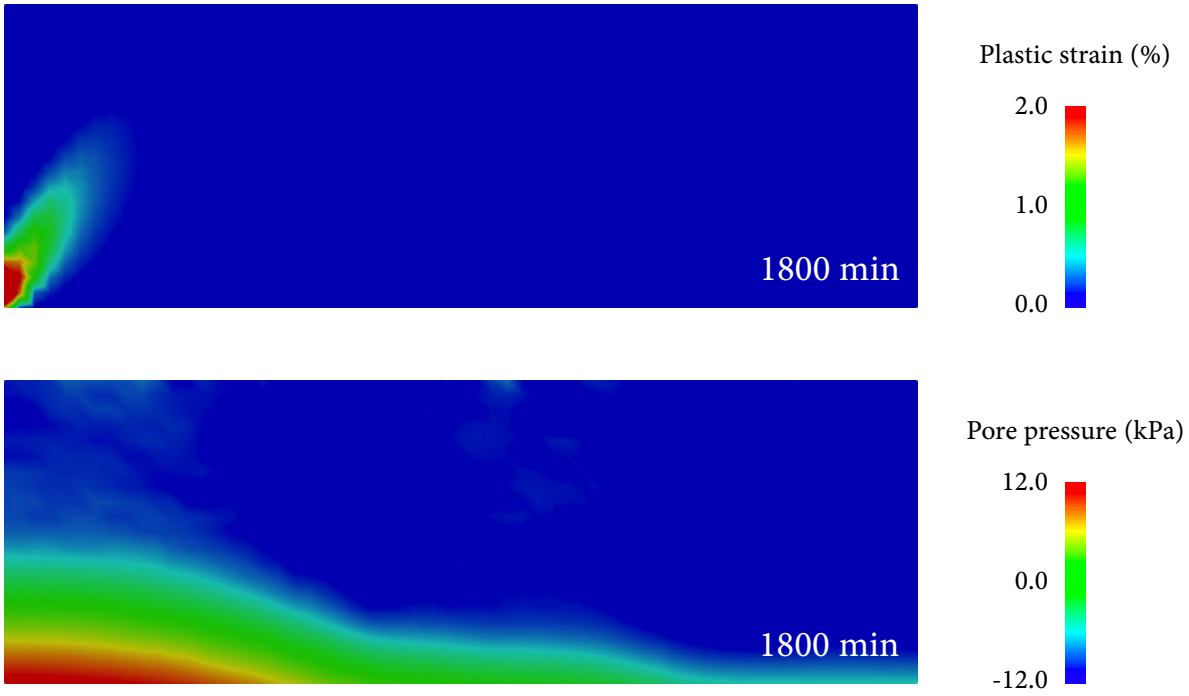

Figure 11: EG solutions of the equivalent plastic strain and pore pressure fields after 1800 minutes.

instance are shown in Fig. 12. The plastic strain in this figure is much less significant than that in the previous one. On a related note, the Newton iteration of the CG simulation converges well until 1980 minutes, at which a plastic zone similar to that in Fig. 11 develops. The reason for this difference can be gleaned from the pore pressure field in the CG solution. In this case, the pore pressure accumulates in the bottom boundary in a nearly uniform manner, so the pressure buildup does not give rise to strain localization at this point. As such, the timing of the wetting collapse predicted by the CG method is about 3 hours later than that by the proposed EG method. To conclude, this example has clearly shown that local mass conservation exerts dominant control not only on the fluid flow but also on the flow-induced deformation in porous media.

5. Closure

We have proposed a finite element formulation for coupled poromechanics that uses the EG method for local mass conservation in the fluid flow. The EG method uses the same bilinear form of the DG method, but its degrees of freedom is appreciably fewer than that of the DG. As such, the proposed formulation allows us to efficiently obtain locally mass conservative solutions with the same order of accuracy of the standard CG methods.

Through numerical examples, we have demonstrated two major reasons why the proposed EG finite element formulation can be an appealing alternative to the conventional CG formulation for coupled poromechanics. First, for problems involving highly heterogeneous permeability fields, the EG formulation can provide non-oscillatory and locally conservative pressure fields whereas the CG formulation cannot. Second, the lack of these capabilities of the CG method can lead to

[3] G. Gambolati, P. Teatini, D. Baú, M. Ferronato, Importance of poroelastic coupling in dynamically active aquifers of the Po river basin, Italy, Water resources research 36 (9) (2000) 2443–2459.
[4] P. Teatini, M. Ferronato, G. Gambolati, M. Gonella, Groundwater pumping and land subsidence in the emilia-romagna coastland, italy: modeling the past occurrence and the future trend, Water Resources Research 42 (1).
[5] R. I. Borja, J. Choo, J. A. White, Rock moisture dynamics, preferential flow, and the stability of hillside slopes, in: Multi-Hazard Approaches to Civil Infrastructure Engineering, 2016, pp. 443–464.
[6] S. Na, W. Sun, Computational thermo-hydro-mechanics for multiphase freezing and thawing porous media in the finite deformation range, Computer Methods in Applied Mechanics and Engineering 318 (2017) 667–700.
[7] M. D. Zoback, Reservoir Geomechanics, Cambridge University Press, 2007.
[8] M. Ferronato, G. Gambolati, C. Janna, P. Teatini, Numerical modelling of regional faults in land subsidence prediction above gas/oil reservoirs, International Journal for Numerical and Analytical Methods in Geomechanics 32 (6) (2008) 633–657.
[9] W. Wang, R. A. Regueiro, J. S. McCartney, Coupled Axisymmetric Thermo-Poro-Mechanical Finite Element Analysis of Energy Foundation Centrifuge Experiments in Partially Saturated Silt, Geotechnical and Geological Engineering 33 (2) (2015) 373–388.
[10] R. Juanes, B. Jha, B. H. Hager, J. H. Shaw, A. Plesch, L. Astiz, J. H. Dieterich, C. Frohlich, Were the May 2012 Emilia-Romagna earthquakes induced? A coupled flow-geomechanics modeling assessment, Geophysical Research Letters 43 (13) (2016) 6891–6897.
[11] B. A. Schrefler, Computer modelling in environmental geomechanics, Computers and Structures 79 (22-25) (2001) 2209–2223.
[12] M. Preisig, J. H. Prévost, Coupled multi-phase thermo-poromechanical effects. Case study: CO_2 injection at In Salah, Algeria, International Journal of Greenhouse Gas Control 5 (4) (2011) 1055–1064.
[13] M. D. Zoback, S. M. Gorelick, Earthquake triggering and large-scale geologic storage of carbon dioxide, Proceedings of the National Academy of Sciences of the United States of America 109 (26) (2012) 10164–10168.
[14] J. Rutqvist, The geomechanics of CO_2 storage in deep sedimentary formations, Geotechnical and Geological Engineering 30 (3) (2012) 525–551.
[15] V. Vilarrasa, O. Silva, J. Carrera, S. Olivella, Liquid CO_2 injection for geological storage in deep saline aquifers, International Journal of Greenhouse Gas Control 14 (2013) 84–96.
[16] J. A. White, L. Chiaramonte, S. Ezzedine, W. Foxall, Y. Hao, A. Ramirez, W. McNab, Geomechanical behavior of the reservoir and caprock system at the In Salah CO_2 storage project, Proceedings of the National Academy of Sciences 111 (24) (2014) 8747–8752.
[17] L. Chiaramonte, J. A. White, W. Trainor-Guitton, Probabilistic geomechanical analysis of compartmentalization at the Snøhvit CO_2 sequestration project, Journal of Geophysical Research: Solid Earth 120 (2) (2015) 1195–1209.
[18] M. A. Celia, Geological storage of captured carbon dioxide as a large-scale carbon mitigation option, Water Resources Research 53 (2017) 3527–3533.
[19] M. A. Murad, A. F. D. Loula, Improved accuracy in finite element analysis of Biot's consolidation problem, Computer Methods in Applied Mechanics and Engineering 95 (3) (1992) 359–382.
[20] M. A. Murad, A. F. Loula, On stability and convergence of finite element approximations of biot's consolidation problem, International Journal for Numerical Methods in Engineering 667 (4) (1994) 645–667.
[21] R. I. Borja, C. Tamagnini, Cam-Clay plasticity, Part III: Extension of the infinitesimal model to include finite strains, Computer Methods in Applied Mechanics and Engineering 155 (1-2) (1998) 73–95.
[22] B. A. Schrefler, R. Scotta, A fully coupled dynamic model for two-phase fluid flow in deformable porous media, Computer Methods in Applied Mechanics and Engineering 190 (24-25) (2001) 3223–3246.
[23] L. Sanavia, B. A. Schrefler, P. Steinmann, A formulation for an unsaturated porous medium undergoing large inelastic strains, Computational Mechanics 28 (2) (2002) 137–151.
[24] J. Wan, Stabilized finite element methods for coupled geomechanics and multiphase flow, Ph.D. thesis, Stanford University (2002).
[25] W. Ehlers, T. Graf, M. Ammann, Deformation and localization analysis of partially saturated soil, Computer Methods in Applied Mechanics and Engineering 193 (27-29) (2004) 2885–2910.
[26] J. E. Andrade, R. I. Borja, Modeling deformation banding in dense and loose fluid-saturated sands, Finite Elements in Analysis and Design 43 (5) (2007) 361–383.

[27] J. A. White, R. I. Borja, Stabilized low-order finite elements for coupled solid-deformation/fluid-diffusion and their application to fault zone transients, Computer Methods in Applied Mechanics and Engineering 197 (49–50) (2008) 4353–4366.
[28] J. A. White, R. I. Borja, Block-preconditioned Newton-Krylov solvers for fully coupled flow and geomechanics, Computational Geosciences 15 (4) (2011) 647–659.
[29] R. A. Regueiro, D. Ebrahimi, Implicit dynamic three-dimensional finite element analysis of an inelastic biphasic mixture at finite strain. Part 1: Application to a simple geomaterial., Computer Methods in Applied Mechanics and Engineering 199 (29-32) (2010) 2024–2049.
[30] M. Preisig, J. H. Prévost, Stabilization procedures in coupled poromechanics problems: A critical assessment, International Journal for Numerical and Analytical Methods in Geomechanics 35 (3) (2011) 1207–1225.
[31] W. Sun, J. T. Ostien, A. Salinger, A stabilized assumed deformation gradient finite element formulation for strongly coupled poromechanical simulations at finite strain, International Journal for Numerical and Analytical Methods in Geomechanics 37 (16) (2013) 2755–2788.
[32] J. Choo, R. I. Borja, Stabilized mixed finite elements for deformable porous media with double porosity, Computer Methods in Applied Mechanics and Engineering 293 (2015) 131–154.
[33] W. Sun, A stabilized finite element formulation for monolithic thermo-hydro-mechanical simulations at finite strain, International Journal for Numerical Methods in Engineering 103 (11) (2015) 798–839.
[34] J. Choo, J. A. White, R. I. Borja, Hydromechanical modeling of unsaturated flow in double porosity media, International Journal of Geomechanics 16 (6) (2016) D4016002.
[35] R. I. Borja, J. Choo, Cam-Clay plasticity, Part VIII: A constitutive framework for porous materials with evolving internal structure, Computer Methods in Applied Mechanics and Engineering 309 (2016) 653–679.
[36] J. A. White, N. Castelletto, H. A. Tchelepi, Block-partitioned solvers for coupled poromechanics: A unified framework, Computer Methods in Applied Mechanics and Engineering 303 (2016) 55–74.
[37] L. Jin, M. D. Zoback, Fully coupled nonlinear fluid flow and poroelasticity in arbitrarily fractured porous media: A hybrid-dimensional computational model, Journal of Geophysical Research: Solid Earth 122 (10) (2017) 7626–7658.
[38] W. Sun, Z. Cai, J. Choo, Mixed Arlequin method for multiscale poromechanics problems, International Journal for Numerical Methods in Engineering 111 (7) (2017) 624–659.
[39] E. Kaasschieter, Mixed finite elements for accurate particle tracking in saturated groundwater flow, Advances in Water Resources 18 (5) (1995) 277–294.
[40] G. Scovazzi, M. F. Wheeler, A. Mikelić, S. Lee, Analytical and variational numerical methods for unstable miscible displacement flows in porous media, Journal of Computational Physics 335 (2017) 444–496.
[41] B. Cockburn, J. Gopalakrishnan, H. Wang, Locally conservative fluxes for the continuous Galerkin method, SIAM Journal on Numerical Analysis 45 (4) (2007) 1742–1776.
[42] S. Sun, M. F. Wheeler, Projections of velocity data for the compatibility with transport, Computer Methods in Applied Mechanics and Engineering 195 (7) (2006) 653–673.
[43] J. Liu, L. Mu, X. Ye, A comparative study of locally conservative numerical methods for darcy's flows, Procedia Computer Science 4 (2011) 974–983.
[44] L. H. Odsæter, M. F. Wheeler, T. Kvamsdal, M. G. Larson, Postprocessing of non-conservative flux for compatibility with transport in heterogeneous media, Computer Methods in Applied Mechanics and Engineering 315 (2017) 799–830.
[45] E. D. do Carmo, M. A. Fernandes, W. J. Mansur, Continuous/discontinuous Galerkin methods applied to elasticity problems, Computer Methods in Applied Mechanics and Engineering 269 (2014) 291–314.
[46] C. Dawson, J. Proft, Coupling of continuous and discontinuous Galerkin methods for transport problems, Computer Methods in Applied Mechanics and Engineering 191 (29) (2002) 3213 – 3231.
[47] J. H. Prévost, Two-way coupling in reservoir–geomechanical models: vertex-centered Galerkin geomechanical model cell-centered and vertex-centered finite volume reservoir models, International Journal for Numerical Methods in Engineering 98 (2014) 612–624.
[48] J. Kim, H. A. Tchelepi, R. Juanes, Stability and convergence of sequential methods for coupled flow and geomechanics: Fixed stress and fixed-strain splits, Computer Methods in Applied Mechanics and Engineering 200 (2011) 1951–1606.

[49] B. Jha, R. Juanes, Coupled multiphase flow and poromechanics: A computational model of pore pressure effects on fault slip and earthquake triggering, Water Resources Research 50.
[50] H. C. Yoon, J. Kim, Spatial stability for the monolithic and sequential methods with various space discretizations in poroelasticity, International Journal for Numerical Methods in Engineering 114 (7) (2018) 694–718.
[51] B. Jha, R. Juanes, A locally conservative finite element framework for the simulation of coupled flow and reservoir geomechanics, Acta Geotechnica 2 (3) (2007) 139–153.
[52] M. Ferronato, N. Castelletto, G. Gambolati, A fully coupled 3-D mixed finite element model of Biot consolidation, Journal of Computational Physics 229 (12) (2010) 4813–4830.
[53] N. Castelletto, G. Gambolati, P. Teatini, A coupled MFE poromechanical model of a large-scale load experiment at the coastland of Venice, Computational Geosciences 19 (1) (2015) 17–29.
[54] N. Castelletto, J. A. White, M. Ferronato, Scalable algorithms for three-field mixed finite element coupled poromechanics, Journal of Computational Physics 327 (2016) 894–918.
[55] R. Liu, M. Wheeler, C. Dawson, R. Dean, Modeling of convection-dominated thermoporomechanics problems using incomplete interior penalty Galerkin method, Computer Methods in Applied Mechanics and Engineering 198 (9–12) (2009) 912–919.
[56] R. Becker, E. Burman, P. Hansbo, M. G. Larson, A reduced P1-discontinuous Galerkin method, Chalmers Finite Element Center Preprint 2003-13.
[57] S. Sun, J. Liu, A locally conservative finite element method based on piecewise constant enrichment of the continuous Galerkin method, SIAM J. Sci. Comput. 31 (2009) 2528–2548.
[58] S. Lee, Y.-J. Lee, M. F. Wheeler, A locally conservative enriched Galerkin approximation and efficient solver for elliptic and parabolic problems, SIAM Journal on Scientific Computing 38 (3) (2016) A1404–A1429.
[59] S. Lee, A. Mikelić, M. F. Wheeler, T. Wick, Phase-field modeling of proppant-filled fractures in a poroelastic medium, Computer Methods in Applied Mechanics and Engineering 312 (2016) 509–541.
[60] S. Lee, M. F. Wheeler, Adaptive enriched Galerkin methods for miscible displacement problems with entropy residual stabilization, Journal of Computational Physics 331 (2017) 19–37.
[61] S. Lee, A. Mikelić, M. Wheeler, T. Wick, Phase-field modeling of two-phase fluid-filled fractures in a poroelastic medium, submitted (2017).
[62] S. Lee, M. F. Wheeler, Enriched Galerkin methods for two-phase flow in porous media with capillary pressure, Journal of Computational Physics 367 (2018) 65–86.
[63] R. I. Borja, Cam-Clay plasticity. Part V: A mathematical framework for three-phase deformation and strain localization analyses of partially saturated porous media, Computer Methods in Applied Mechanics and Engineering 193 (48-51) (2004) 5301–5338.
[64] R. I. Borja, On the mechanical energy and effective stress in saturated and unsaturated porous continua, International Journal of Solids and Structures 43 (6) (2006) 1764–1786.
[65] J. C. Simo, T. J. R. Hughes, Computational Inelasticity, Springer Berlin Heidelberg, 1998.
[66] E. A. de Souza Neto, D. Peric, D. R. J. Owen, Computational Methods for Plasticity: Theory and Applications, John Wiley & Sons, 2008.
[67] R. I. Borja, Plasticity Modeling and Computation, Springer Berlin Heidelberg, 2013.
[68] M. Th. van Genuchten, A closed-form equation for predicting the hydraulic conductivity of unsaturated soils, Soil Science Society of America 44 (5) (1980) 892–898.
[69] J. H. Prévost, Nonlinear transient phenomena in saturated porous media, Computer Methods in Applied Mechanics and Engineering 30 (1) (1982) 3–18.
[70] O. Zienkiewicz, T. Shiomi, Dynamic behaviour of saturated porous media; The generalized Biot formulation and its numerical solution, International Journal for Numerical and Analytical Methods in Geomechanics 8 (1) (1984) 71–96.
[71] P. G. Ciarlet, The Finite Element Method for Elliptic Problems, North-Holland, 1978.
[72] A. Ern, A. F. Stephansen, P. Zunino, A discontinuous Galerkin method with weighted averages for advection–diffusion equations with locally small and anisotropic diffusivity, IMA Journal of Numerical Analysis 29 (2) (2009) 235–256.
[73] S. Sun, M. F. Wheeler, Discontinuous Galerkin methods for coupled flow and reactive transport problems, Applied Numerical Mathematics 52 (2) (2005) 273–298.

[74] S. Sun, M. F. Wheeler, Symmetric and nonsymmetric discontinuous Galerkin methods for reactive transport in porous media, SIAM Journal on Numerical Analysis 43 (1) (2005) 195–219.
[75] B. Riviere, M. F. Wheeler, V. Girault, A priori error estimates for finite element methods based on discontinuous approximation spaces for elliptic problems 39 (3) (2001) 902–931.
[76] K. Shahbazi, An explicit expression for the penalty parameter of the interior penalty method, Journal of Computational Physics 205 (2) (2005) 401 – 407.
[77] Y. Epshteyn, B. Riviére, Estimation of penalty parameters for symmetric interior penalty Galerkin methods, Journal of Computational and Applied Mathematics 206 (2) (2007) 843–872.
[78] M. Ainsworth, R. Rankin, Technical note: A note on the selection of the penalty parameter for discontinuous galerkin finite element schemes, Numerical Methods for Partial Differential Equations 28 (3) (2012) 1099–1104.
[79] J. Choo, Hydromechanical modeling framework for multiscale porous materials, Ph.D. thesis, Stanford University (2016).
[80] C. Taylor, P. Hood, A numerical solution of the Navier–Stokes equations using the finite element technique, Computers & Fluids 1 (1) (1973) 73–100.
[81] D. Boffi, N. Cavallini, F. Gardini, L. Gastaldi, Local mass conservation of Stokes finite elements, Journal of Scientific Computing 52 (2) (2012) 383–400.
[82] M. Celia, E. T. Bouloutas, R. L. Zarba, A general mass-conservative numerical soluition for the unsaturated flow equation, Water Resources Research 26 (1) (1990) 1483–1496.
[83] A. Mikelić, M. F. Wheeler, Convergence of iterative coupling for coupled flow and geomechanics, Computational Geosciences 17 (3) (2013) 455–461.
[84] W. Bangerth, R. Hartmann, G. Kanschat, deal . II—A general-purpose object-oriented finite element library 33 (4) (2007) 1–27.
[85] D. Arndt, W. Bangerth, D. Davydov, T. Heister, L. Heltai, M. Kronbichler, M. Maier, J.-P. Pelteret, B. Turcksin, D. Wells, The `deal.II` library, version 8.5, Journal of Numerical Mathematics 25 (3) (2017) 137–146.
[86] C. Burstedde, L. C. Wilcox, O. Ghattas, p4est: Scalable algorithms for parallel adaptive mesh refinement on forests of octrees, SIAM Journal on Scientific Computing 33 (3) (2011) 1103–1133.
[87] M. A. Heroux, J. M. Willenbring, A new overview of the Trilinos project, Scientific Programming 20 (2) (2012) 83–88.
[88] D. C. Drucker, W. Prager, Soil mechanics and plastic analysis for limit design, Quarterly of Applied Mathematics 10 (2) (1952) 157–165.
[89] J. Choo, W. Sun, Coupled phase-field and plasticity modeling of geological materials: From brittle fracture to ductile flow, Computer Methods in Applied Mechanics and Engineering 330 (2018) 1–32.
[90] A. J. Abbo, S. W. Sloan, A smooth hyperbolic approximation to the Mohr-Coulomb yield criterion, Computers and Structures 54 (3) (1995) 427–441.
[91] Y. L. Young, J. A. White, H. Xiao, R. I. Borja, Liquefaction potential of coastal slopes induced by solitary waves, Acta Geotechnica 4 (1) (2009) 17–34.
[92] R. I. Borja, J. A. White, Continuum deformation and stability analyses of a steep hillside slope under rainfall infiltration, Acta Geotechnica 5 (1) (2010) 1–14.
[93] C. Miehe, S. Mauthe, Phase field modeling of fracture in multi-physics problems. Part III. Crack driving forces in hydro-poro-elasticity and hydraulic fracturing of fluid-saturated porous media, Computer Methods in Applied Mechanics and Engineering 304 (2015) 619–655.
[94] S. Lee, A. Mikelić, M. F. Wheeler, T. Wick, Phase-field modeling of proppant-filled fractures in a poroelastic medium, Computer Methods in Applied Mechanics and Engineering 312 (2016) 509–541.
[95] S. Lee, M. F. Wheeler, T. Wick, Pressure and fluid-driven fracture propagation in porous media using an adaptive finite element phase field model, Computer Methods in Applied Mechanics and Engineering 305 (2016) 111–132.
[96] Z. A. Wilson, C. M. Landis, Phase-field modeling of hydraulic fracture, Journal of the Mechanics and Physics of Solids 96 (2016) 264–290.
[97] S. Lee, M. F. Wheeler, T. Wick, Iterative coupling of flow, geomechanics and adaptive phase-field fracture including level-set crack width approaches, Journal of Computational and Applied Mathematics 314 (2017) 40–60.
[98] K. Wang, W. Sun, A unified variational eigen-erosion framework for interacting brittle fractures and compaction bands in fluid-infiltrating porous media, Computer Methods in Applied Mechanics and Engineering 318 (2017)

1–32.
[99] J. Choo, W. Sun, Cracking and damage from crystallization in pores: Coupled chemo-hydro-mechanics and phase-field modeling, Computer Methods in Applied Mechanics and Engineering 335 (2018) 347–379.
[100] S. J. Ha, J. Choo, T. S. Yun, Liquid CO_2 fracturing: Effect of fluid permeation on the breakdown pressure and cracking behavior, submitted (2018).

View publication stats